Controlled formation of Schottky diodes on n-doped ZnO layers by deposition of p-conductive polymer layers with oxidative chemical vapor deposition

NANO EXPRESS

PAPER

Controlled formation of Schottky diodes on n-doped ZnO layers by deposition of p-conductive polymer layers with oxidative chemical vapor deposition

Linus Krieg[1], **Zhipeng Zhang**[2], **Daniel Splith**[2], **Holger von Wenckstern**[2], **Marius Grundmann**[2], **Xiaoxue Wang**[3], **Karen K Gleason**[3] and **Tobias Voss**[1]

[1] Institute of Semiconductor Technology and Laboratory of Emerging Nanometrology, Technische Universität Braunschweig, Langer Kamp 6a/b, 38106 Braunschweig, Germany
[2] Felix-Bloch-Institut für Festkörperphysik, University Leipzig, Linnéstr. 5, 04013 Leipzig, Germany
[3] Department of Chemical Engineering, Massachusetts Institute of Technology, 02139 Cambridge, MA, United States of America

E-mail: tobias.voss@tu-braunschweig.de

Keywords: ZnO, PEDOT, inorganic-organic interfaces, oCVD

OPEN ACCESS

RECEIVED
8 January 2020

REVISED
19 March 2020

ACCEPTED FOR PUBLICATION
24 March 2020

PUBLISHED
7 April 2020

Abstract

We report the controlled formation of organic/inorganic Schottky diodes by depositing poly(3,4-ethylenedioxythiophene) (PEDOT) on n-doped ZnO layers using oxidative chemical vapor deposition (oCVD). Current-voltage measurements reveal the formation of Schottky diodes that show good thermal and temporal stability with rectification ratios of 10^7 and ideality factors of ~1.2. In the frame of a Schottky model, we identify a mean barrier height at the hybrid inorganic-organic interface of 1.28 eV, which is consistent with the difference between the work function of PEDOT and the electron affinity of ZnO. The findings highlight the strength of oCVD to design high-quality hybrid PEDOT/ZnO heterojunctions with possible applications in electronic and optoelectronic devices.

1. Introduction

ZnO is a widely analyzed material that features useful properties which makes it an excellent base for applications in various fields that range from supercapacitors to energy storage or biosensors [1]. Due to its direct and wide bandgap and the simplicity of n-type doping, ZnO is especially suitable for UV optoelectronic applications [2]. However, stable and reproducible p-type doping of ZnO has not been achieved, which limits the use of ZnO to unipolar devices. To overcome this challenge, hole conductive organic materials can be used to form diode-like heterostructures with n-doped ZnO layers. Advantages of conducting polymers comprise their chemical and mechanical stability in combination with a high degree of flexibility and processability at ambient temperatures [3]. One very promising polymer is poly(3,4-ethylenedioxythiophene) (PEDOT), which is hole-conductive, has reported conductivities >6000 S cm^{-1} [4], is largely transparent in the visible spectral range and highly flexible [5]. Among many other applications, PEDOT is already used in transparent electrodes [3], in energy conversion and storage devices [6] or for thermoelectrics [7].

One drawback of PEDOT is its hydrophobic nature and insolubility in water [8] which hinders growth by commonly used liquid-based deposition techniques. By adding an anionic polyelectrolyte to stabilize the otherwise insoluble PEDOT in aqueous environments, the water-soluble PEDOT:PSS (PSS: polystyrene sulfonate) can be obtained. The additive mostly used is the insulating PSS which leads to an energy barrier for charge transport in the film [3]. In addition, due to the high acidity of PEDOT:PSS, strong etching effects are expected on many surfaces like ZnO in acidic environments.

Hybrid structures consisting of inorganic ZnO and organic PEDOT:PSS are under investigation in several fields. On the one hand, PEDOT:PSS deposited on ZnO leads to the formation of diodes [9–12], on the other hand, hybrid nanocomposites for sensing applications or optoelectronics are in the center of attention [2, 13].

However, for hybrid heterojunctions based on spin-coated PEDOT:PSS on ZnO, etching effects have to be taken into account. In particular, substantial densities of defect states are likely to be introduced at the organic/

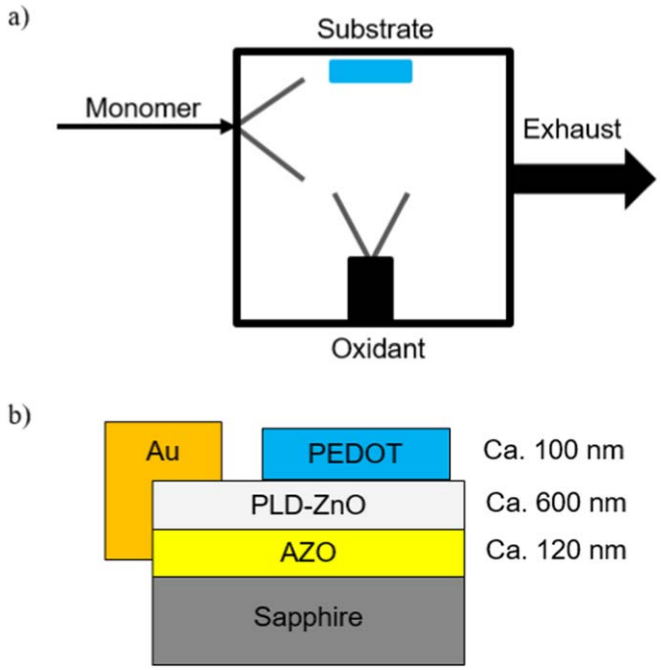

Figure 1. (a) Sketch of an oCVD reactor; (b) cross-section of the sample design.

inorganic interface that, e.g., show up as green-to-orange light-emitting centers in hybrid LEDs [14, 15]. To circumvent etching of the inorganic material and the reduced inhomogeneous conductivity associated with the insulating PSS domains in the organic layer, deposition techniques from the gas phase can be applied. Especially oxidative chemical vapor deposition (oCVD) is a suitable tool [16, 17], as the polymer is deposited directly from the gas phase and contact of solvents and the ZnO substrate can be avoided. This promises to lead to more defined and defect-free interfaces. In addition, PEDOT can be used in its pure state without the additive PSS thus improving the conductivity of the organic film and its homogeneity. Furthermore, the PEDOT film is *in situ* p-doped during the growth process which leads directly to the formation of a hybrid organic/inorganic p-n junction.

We use oCVD to deposit p-type PEDOT on n-type ZnO layers grown by pulsed laser deposition (PLD). Current-voltage measurements at room temperature reveal a clear diode behavior with rectification ratios of 10^7 and ideality factors $n < 1.3$. The hybrid heterojunctions show good thermal and temporal stability. Applying the model of a laterally inhomogeneous electronic barrier height at the hybrid interface in the frame of a Schottky model allows for the determination of a mean barrier height of $\Phi_{B0,m} = (1.28 \pm 0.01)$ eV. This is consistent with the homogeneous barrier height determined by the model of patchy contacts and the difference between the work function of the metal and the electron affinity of the semiconductor. Together the findings support the claim of thermionic emission as the leading conduction mechanism at the hybrid interface.

2. Materials and methods

ZnO layers were grown on sapphire substrates using pulsed layer deposition (PLD). As a laser, a KrF excimer laser with a wavelength of 248 nm and a repetition rate of 15 Hz with an energy density of about 2 J cm^{-2} is used. The target to substrate distance was kept at 10 cm, substrate temperature at 640 °C and the oxygen partial pressure at 0.02 mbar. Details of the PLD process are described by Lorenz *et al* [18].

oCVD was performed using a home-built reactor (figure 1(a)). In brief, the monomer, in the case of this work EDOT (3,4-ethylenedioxythiophene, purchased from Sigma Aldrich) is introduced into the vacuum chamber at base pressures of 10^{-2} to 10^{-7} mbar. The substrate is mounted on a heated stage face-down at the top of the chamber. From below, an oxidizing agent is co-sublimated to the inserted monomer vapor. As long as the oxidizing agent is provided, the polymerization process persists and doped polymer films are conformally deposited onto the substrate surface. A post-deposition rinsing step removes reaction byproducts. Details of the oCVD process can be found in [4, 19].

The resulting sample is sketched in figure 1(b). It consists of a sapphire substrate with a thin, 120 nm AZO layer with an estimated charge carrier concentration of 10^{19} cm^{-3}. The AZO layer serves as a back contact to realize a truly vertical diode structure. On top of the AZO layer, nominally undoped PLD ZnO was deposited

with a thickness of about 600 nm. The PLD ZnO and AZO film thickness was estimated from the growth rate determined by ellipsometry on different thin films grown under the same conditions. The charge carrier concentration at the surface is anticipated to be $\sim 10^{16}$ cm^{-3} [20]. Before the deposition of the PEDOT layer, a photolithographic mask was placed on the surface, which provided uncovered circular PLD-ZnO areas with well-defined diameters from 150 μm up to 750 μm. PEDOT was deposited using oCVD with a substrate temperature of 400 K, a deposition time of 25 min and $FeCl_3$ as oxidizing agent. To remove residual chemicals, a post-deposition rinsing step with MeOH was applied. The rinsing step also dissolved the photolithographic mask. Therefore, after the deposition and rinsing, well-defined PEDOT patches are located on the PLD-ZnO. Finally, Au was deposited on the edge of the sample contacting PLD-ZnO and the AZO layer as an ohmic back-contact. We note that two additional samples were designed with deposition times of 10 and 15 min resulting in film thicknesses of 40 and 70 nm, respectively. Here, we restrict ourselves to the evaluation of the thickest sample with a PEDOT layer of 100 nm (deposition time: 25 min) as no significant differences in the electronic properties among the three samples were detected. The film thickness of the PEDOT layer was determined using Atomic Force Microscopy (AFM) on a reference wafer that was placed inside the oCVD reactor during the growth process.

Due to the use of $FeCl_3$ as the oxidant, both Fe and Cl could in principle diffuse into the ZnO lattice at the initial stage of the oCVD process when the bare ZnO surface is exposed to the gases in the reactor. In particular, the diffusion of Fe ions into the ZnO lattice would lead to additional deep level defects in ZnO with substantial implications for the optical and electrical characteristics of the later device [21–23]. However, due to the quite low substrate temperature, we expect interdiffusion processes to be negligible. In addition, surface-sensitive XPS and EDX measurements on a PEDOT/organic substrate interface in earlier studies showed no or low Fe signals originating from the PEDOT layer after a comparable rinsing step to the one carried out for the samples analyzed here [24, 25]. We, therefore, conclude that any incorporation of Fe into the ZnO lattice does not affect its properties to a large extent in our experiments.

Electrical characterizations were performed in darkness using a Süss Waferprober system P200 connected to a semiconductor parameter analyzer (Agilent 4155C). For the temperature-dependent measurements, the sample was heated starting at room temperature with a maximum temperature of 423 K. After reaching the maximum temperature, the sample was cooled down to room temperature again. For every data point obtained during heating and cooling, the temperature was kept stable for 3 min prior to data acquisition.

3. Results and discussions

3.1. Electrical characterization

To determine the electrical characteristics of the hybrid interface, current-voltage measurements were performed. A clear diode behavior of the hybrid structure is revealed (figure 2). Rectification ratios of up to 10^7 at $+/-2$ V were routinely obtained. These are comparable to the rectifications reported in the literature so far [9, 10]. The large rectification ratios persisted even after storing the sample for more than 25 weeks in darkness in air whilst the series resistance increased during the storage time. The rectification is fully attributed to the hybrid heterojunction as current-voltage measurements of the pure PEDOT layer and the Au/AZO back-contact revealed ohmic behavior (measurements not shown). After 25 weeks, the sample was heated to 423 K to test the temperature stability of the sample. The annealing of the sample leads to a larger reverse current density and a reduced current density in forward direction between 0.5 and 3 V (figure 2). Therefore, temperature-induced changes must be taken into account. According to Lee *et al* [25], temperature-induced changes in oCVD-PEDOT can originate from the formation of $Fe(OH)_2$ complexes as a result of dedoping reactions in the presence of water and oxygen.

3.2. Schottky model

oCVD-PEDOT has been reported to show metallic behavior [4]. Therefore, the electrical characteristics can be analyzed in the frame of a Schottky model where the current I can be described as

$$I = I_s\left(\exp\left(\frac{e(U - R_s I)}{k_B T n}\right) - 1\right) + \frac{U - R_s I}{R_p}. \quad (1)$$

U is the applied voltage, R_s is the series resistance, R_p is the parallel resistance accounting for shunts, k_B and e are the Boltzmann constant and the elementary charge, respectively. n is the ideality factor reflecting the bias dependence of the barrier height and allowing to deduce the quality of the diode. Values close to 1 describe an ideal diode, whilst values larger than 1 can be attributed to defects or an inhomogeneous distribution of barrier heights at the electrical interface as discussed by Werner and Güttler [26]. I_s is the saturation current which can be written as:

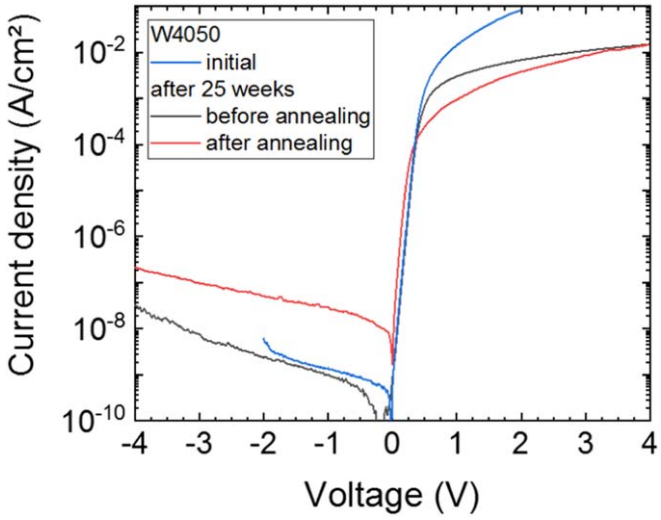

Figure 2. Current density plotted as a function of the applied voltage. The strong rectifying behavior of the device persists after storage of 25 weeks in dark under ambient conditions and annealing the sample at 423 K.

$$I_s = A_0 A\ T^2 \exp\left(\frac{-\phi_{B,eff}}{k_B T}\right). \tag{2}$$

A_0 is the contact area, A the effective Richardson constant ($A = 32\ \mathrm{A\,cm^{-2}\,K^{-2}}$ for ZnO with an effective electron mass of 0.27 m_0 [20]), T the temperature, and $\Phi_{B,eff}$ the effective Schottky barrier height of the diode.

Fitting equation (1) to the linear region in forward direction on a semilogarithmic scale of the *I-V* curve for the initial measurement in figure 2 (blue) yields an ideality factor of $n = 1.1$ and an effective barrier height of $\Phi_{B,eff} = 0.94$ eV. We note, that the PEDOT film thickness for values of 40, 70 and 100 nm did not show any significant influence on neither rectification ratio, nor effective barrier height nor ideality factor. This strengthens our assumption of quasi-metallic conductivity in the PEDOT layer and the analysis of the hybrid heterojunction as a one-sided diode. The depletion zone of the Schottky contact can be found in the n-GaN and the film thickness of the PEDOT, therefore, influences rather the series resistance than the electronic properties of the interface.

The obtained values of the ideality factor and the effective barrier height are in the order of the earlier reported values of Nakano *et al* for a structure consisting of PEDOT:PSS deposited on ZnO via spin-coating [9]. Nakano *et al* reported an ideality factor of $n = 1.02$ and an effective barrier height of $\Phi_{B,eff} = 1.1$ eV.

According to the model of potential fluctuation of Schottky barriers by Werner and Güttler [26], the effective barrier height shows a characteristic temperature dependence. Werner *et al* assume, that the effective barrier at the interface is inhomogenous which can be described by a Gaussian distribution of effective barrier heights at the interface with a standard deviation σ:

$$\phi_{B,eff}(T) = \phi_{B0,m} - \frac{\sigma^2}{2k_B T}. \tag{3}$$

$\Phi_{B0,m}$ is the mean barrier height at the hybrid interface at zero bias and can be determined by a plot of the effective barrier heights as a function of the inverse temperature (figure 3). The values were obtained while cooling down the sample from 423 K back to room temperature.

The effective barrier height shows the expected dependence on temperature and becomes smaller with decreasing temperature from values of $\Phi_{B,eff}(T = 423\ \mathrm{K}) = 0.97$ eV to $\Phi_{B,eff}(T = 293\ \mathrm{K}) = 0.84$ eV. The linear fit according to equation (3) yields a mean barrier height of $\Phi_{B0,m} = (1.28 \pm 0.01)$ eV and a standard deviation of $\sigma = (151 \pm 17)$ meV.

In addition, figure 3 shows the ideality factor over the inverse temperature. We find only small variations of the ideality factor $n = 1.1 \pm 0.05$ with the temperature within the studied temperature range thus emphasizing that thermally activated processes with activation energies in the range of 25–40 meV play only a minor role for the hybrid heterojunctions.

The determination of ideality factors and effective barrier heights was performed for several diodes on the sample before the annealing process. In figure 4, we plot the effective barrier height as a function of the ideality factor. As can be seen for the different diodes at room temperature (blue), the effective barrier height shows a narrow distribution around (0.93 ± 0.02) eV with few exceptions whilst the ideality factor varies between 1.1

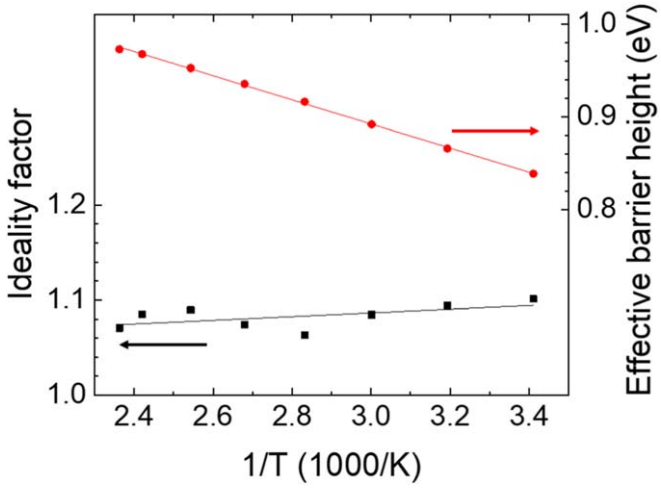

Figure 3. Ideality factor and effective barrier height as obtained from current-voltage measurements using a Schottky diode model. Linear fitting of the effective barrier heights allows for the determination of the mean barrier height according to the model of Werner and Güttler.

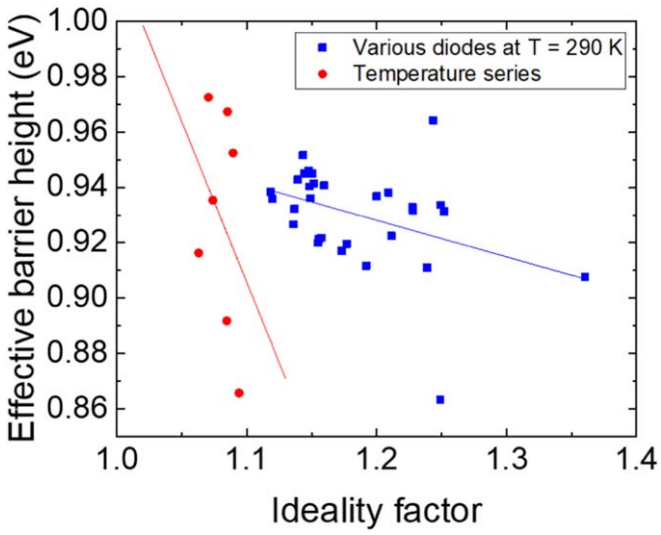

Figure 4. Dependence of the effective barrier height on the ideality factor. In blue, data points received for various diodes before annealing the sample at 423 K are shown. Red data points were obtained for a single diode during the cooling process from 423 K to 293 K. Linear interpolation to n = 1.02 allows for the determination of the homogenous barrier height.

and 1.3. This is different from the values obtained for the temperature series where the ideality factor is basically constant but shows a constant temperature-induced change of the effective barrier heights.

Schmitsdorf *et al* [27] deduce from the dependence of the effective barrier height on the ideality factor the homogeneous barrier height $\varphi_{B0,h}$. Their approach is based on an empirical model of Tung *et al* [28]. In principle, the interface is described as 'patchy' with patches of reduced effective barrier height that are embedded in a matrix with a homogenous electronic barrier. The size of these patches is comparable with or even smaller than the Debye length. This homogenous electronic barrier can be determined by linear interpolation of the effective barrier height to an ideality factor of 1.02, which represents the ideality factor of an ideal diode, where only image-force barrier lowering needs to be considered. The homogenous barrier height as determined by linear interpolation to the effective barriers of multiple different diodes (figure 4, blue) yields a value of $\varphi_{B0,h} = (0.95 \pm 0.18)$ eV. For a single diode measured at different temperatures, the ideality factor is close to constant (figure 4, red). Therefore a linear interpolation over the ideality factor gives just a rough estimation for the homogenous barrier height of $\varphi_{B0,h} \sim 1.00$ eV and a large error has to be taken into account.

Table 1 summarizes the obtained values of the ideality factor as well as the mean barrier height and the homogeneous barrier height. The homogeneous barrier height is roughly 300 meV lower than the value for the

Table 1. Comparison of the parameters obtained using different Schottky models.

		$\Phi_{B0,h}$ [eV]	
Ideality factor (T = 293 K)	$\Phi_{B0,m}$ [eV]	Multiple diodes	Single diode at various T
1.2 ± 0.1	1.28 ± 0.01	0.95 ± 0.18	~1.00

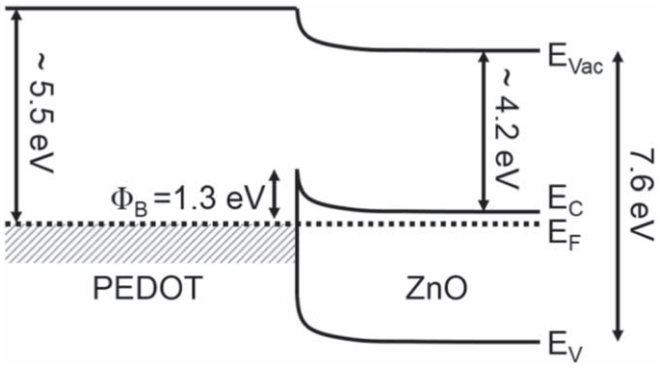

Figure 5. Schematic band diagram of the hybrid interface.

mean barrier height in the model of Werner and Güttler. This can be explained with the more empirical nature of the approach by Schmitsdorf *et al* as compared to the theoretically guided model by Werner and Güttler.

Figure 5 summarizes the findings of this work in a simplified band structure. The value of the work function for oCVD PEDOT depends on the substrate temperature during the deposition process and is estimated according to Im *et al* as 5.5 eV [19]. The electron affinity and bandgap of ZnO are reported to be 4.2 eV [29] and 3.37 eV [30], respectively. The mean barrier height determined by the model of a fluctuating potential at the hybrid interface matches well the difference between the work function of oCVD PEDOT and the electron affinity of ZnO. This is the expected behavior for a metal-semiconductor Schottky contact [31].

Overall, our results provide a consistent model of the hybrid PEDOT/n-ZnO interface and demonstrate nearly ideal Schottky characteristics. In addition, the use of oCVD as a deposition method from the gas phase allows for the use of pure PEDOT and features the potential of homogeneous coatings of nano- and microstructured ZnO-templates as well as industrial scale-up. Thus, the results constitute a significant step towards applications of hybrid PEDOT/n-ZnO structures in electronic and optoelectronic applications.

4. Conclusion

In summary, we have studied the formation of hybrid organic/inorganic Schottky diodes consisting of oCVD p-PEDOT and n-ZnO and analyzed their electronic properties. Rectification ratios are in the order of 10^7 and show good thermal and temporal stabilities. Using a Schottky model allows for the determination of ideality factors and effective barrier heights. The ideality factors are in the order of 1.1 which signifies low contributions of defects to the diode characteristics thus a low defect density at the interface. Therefore, oCVD has proven to be a suitable tool to coat the chemically fragile ZnO surface with PEDOT as an alternative to solvent-based deposition techniques. Taking the determined effective barrier heights allows for the estimation of the mean barrier height within the model of a fluctuating potential at the hybrid interface. The mean barrier height of 1.28 eV matches the difference between the work function of PEDOT and the electron affinity of ZnO reported in literature perfectly. Together, the findings strengthen the idea of oCVD PEDOT to be seen as metallic and the hybrid organic/inorganic interface as a Schottky contact with a predominant thermionic emission as conduction mechanism. Applications of such interfaces in optoelectronics or sensors might be possible.

Acknowledgments

We thank Holger Hochmuth for the masking and preparation of the ZnO substrates. We acknowledge financial support from 'Niedersächsisches Vorab' through 'Quantum- and Nano-Metrology (QUANOMET)' initiative

within the project NL-3 'Sensors'. We gratefully acknowledge support by the Deutsche Forschungsgemeinschaft (DFG, German Research Foundation) Research Training Group GrK1952/2 'Metrology for Complex Nanosystems' and the Braunschweig International Graduate School of Metrology B-IGSM. This work has been supported by the DFG within the research unit FOR1616. Funded by the Deutsche Forschungsgemeinschaft under Germany's Excellence Strategy—EXC-2123 QuantumFrontiers—390837967. M G, H v W and D S acknowledge funding by the European Social Fund within the Young Investigator Group 'Oxide Heterostructures' (SAB 100310460).

Data availability

The data that support the findings of this study are available upon request from the authors.

ORCID iDs

Linus Krieg https://orcid.org/0000-0002-0196-1263
Daniel Splith https://orcid.org/0000-0001-5434-2194
Holger von Wenckstern https://orcid.org/0000-0002-3936-275X
Marius Grundmann https://orcid.org/0000-0001-7554-182X
Tobias Voss https://orcid.org/0000-0003-2580-2723

References

[1] Theerthagiri J, Salla S, Senthil R A, Nithyadharseni P, Madankumar A, Arunachalam P, Maiyalagan T and Kim H-S 2019 *Nanotechnology* **30** 392001
[2] Voss T and Waldvogel S R 2016 *Mater. Sci. Semicond. Process.* **69** 52–6
[3] Hofmann A I, Cloutet E and Hadziioannou G 2018 *Adv. Electron. Mater.* **4** 1700412
[4] Wang X, Zhang X, Sun L, Lee D, Lee S, Wang M, Zhao J, Shao-Horn Y, Dinca M, Palacios T and Gleason K K 2018 *Sci. Adv.* **4** 1–9
[5] Kayser L V and Lipomi D J 2019 *Adv. Mater.* **31** 1–13
[6] Sun K, Zhang S, Li P, Xia Y, Zhang X, Du D, Isikgor F H and Ouyang J 2015 *J. Mater. Sci. Mater. Electron.* **26** 4438–62
[7] Zheng Y, Zeng H, Zhu Q and Xu J 2018 *J. Mater. Chem.* C **6** 8858–73
[8] Yano H, Kudo K, Marumo K and Okuzaki H 2019 *Sci. Adv.* **5** 1–10
[9] Nakano M *et al* 2008 *Appl. Phys. Lett.* **93** 1–4
[10] Nakano M, Tsukazaki A, Gunji R Y, Ueno K, Ohtomo A, Fukumura T and Kawasaki M 2007 *Appl. Phys. Lett.* **91** 2005–8
[11] Yang Q, Liu Y, Pan C, Chen J, Wen X and Wang Z L 2013 *Nano Lett.* **13** 607–13
[12] Paul S, Harris P G, Sharma A K and Ray A K 2018 *J. Mater. Sci. Mater. Electron.* **29** 2797–805
[13] Harikrishnan G, Vempati S, Prajapati K N, Bandopadhyay K, Kalathingal V and Mitra J 2019 *Nanoscale Adv.* **1** 2435–43
[14] Könenkamp R, Word R C and Schlegel C 2004 *Appl. Phys. Lett.* **85** 6004–6
[15] Dev A, Elshaer A and Voss T 2011 *IEEE J. Sel. Top. Quantum Electron.* **17** 896–906
[16] Heydari Gharahcheshmeh M and Gleason K K 2019 *Adv. Mater. Interfaces* **6** 1–27
[17] Gharahcheshmeh M H, Tavakoli M M, Gleason E F, Robinson M T, Kong J and Gleason K K 2019 *Sci. Adv.* **5** 1–13
[18] Lorenz M, Wagner G, Rahm A, Schmidt H, Hochmuth H, Schmid H, Mader W, Brandt M, Von Wenckstern H and Grundmann M 2008 *Phys. Status Solidi Curr. Top. Solid State Phys.* **5** 3280–7
[19] Im S G and Gleason K K 2007 *Macromolecules* **40** 6552–6
[20] Von Wenckstern H, Biehne G, Rahman R A, Hochmuth H, Lorenz M and Grundmann M 2006 *Appl. Phys. Lett.* **88** 23–5
[21] Ivanovski V N, Belošević-Čavor J, Rajić V, Umićević A, Marković S, Kusigerski V, Mitrić M and Koteski V 2019 *J. Appl. Phys.* **126** 125703
[22] Malguth E, Hoffmann A and Phillips M R 2008 *Phys. Status Solidi Basic Res.* **245** 455–80
[23] Klingshirn C F, Meyer B K, Waag A, Hoffmann A and Geurts J 2010 *Zinc Oxide - From Fundamental Properties Towards Novel Applications* (Berlin Heidelberg: Springer-Verlag)
[24] Im S G, Gleason K K and Olivetti E A 2007 *Appl. Phys. Lett.* **90** 88–91
[25] Lee S, Paine D C and Gleason K K 2014 *Adv. Funct. Mater.* **24** 7187–96
[26] Werner J H and Güttler H H 1991 *J. Appl. Phys.* **69** 1522
[27] Schmitsdorf R F, Kampen T U and Mönch W 1997 *J. Vac. Sci. Technol. B Microelectron. Nanom. Struct. Process. Meas. Phenom.* **15** 1221–6
[28] Tung R T 1992 *Phys. Rev.* B **45** 13509–23
[29] Brillson L J and Lu Y 2011 *J. Appl. Phys.* **109** 121301
[30] Klingshirn C F 2007 *Chem. Phys. Chem.* **8** 782–803
[31] Grundmann M 2006 *The Physics of Semiconductors—An Introduction Including Devices and Nanophysics* (Berlin Heidelberg: Springer-Verlag)